Newly Assembled Microtubules Are Concentrated in the Proximal and Distal Regions of Growing Axons

Anthony Brown, Theresa Slaughter, and Mark M. Black

Department of Anatomy and Cell Biology, Temple University School of Medicine, Philadelphia, Pennsylvania 19140

Abstract. We have investigated the sites of microtubule (MT) assembly in neurons during axon growth by taking advantage of the relationship between the proportion of tyrosinated α-tubulin (tyr-tubulin) in MTs and their age. Specifically, young (newly assembled) MTs contain more tyr-tubulin than older (more long-lived) MTs. To quantify the relative proportion of tyr-tubulin in MTs, cultured rat sympathetic neurons were permeabilized under conditions that stabilize existing MTs and remove unassembled tubulin. The MTs were then double-stained with antibodies to tyr-tubulin (as a measure of the amount of tyr-tubulin in MTs) and to β-tubulin (as a measure of total MT mass), using immunofluorescence procedures. Cells were imaged with a cooled charge-coupled device camera and the relative proportion of tyr-tubulin in the MTs was quantified by computing the ratio of the tyr-tubulin fluorescence to the β-tubulin fluorescence using a novel application of digital image processing and analysis techniques. The amount of tyr-tubulin in the MTs was highest in the cell body and at the growth cone; peak ratios in these two regions were ~10-fold higher than for the axon shaft. Moving out from the cell body into the axon, the tyr-tubulin content declined over an average distance of 40 μm to reach a constant low value within the axon shaft and then rose again more distally, over an average distance of 110 μm, to reach a peak at the growth cone (average axon length = 358 μm). These observations indicate that newly assembled MTs are concentrated in the proximal and distal regions of growing axons and therefore that the cell body and growth cone are the most active sites of MT assembly dynamics in neurons that are actively extending axons.

During axon growth there is an increase in the number and length of microtubules (MTs)[1] in the axon (Jacobs and Stevens, 1986). However, the principal sites of assembly of axonal MTs have not been identified. In the *Structural Hypothesis of Axonal Transport*, it was proposed that axonal cytoskeletal polymers (MTs, neurofilaments and microfilaments) are assembled in the cell body and are transported into and along the axon throughout the life of the neuron (Tytell et al., 1981; Lasek, 1986, 1988). According to this hypothesis, the cell body is the principal site of formation of axonal cytoskeletal polymers and the transport of these polymers into and along the axon is the principal mechanism for the addition of new axonal cytoskeleton to the growing axon.

Recent support for the movement of MTs in axons has come from direct observations on axonal MTs in living embryonic *Xenopus* neurons using photoactivation of caged fluorescent tubulin (Reinsch et al., 1991). Microtubule translocation towards the growth cone was observed at all points along the axon and this supports the hypothesis that the cell body is a site of new polymer assembly for the axon. However, studies on PC12 cells and mouse dorsal root ganglion neurons using laser photobleaching of fluorescent tubulin have not detected any directional movement of axonal tubulin (Lim et al., 1989, 1990; Okabe and Hirokawa, 1990). These results, which appear to conflict with those of Reinsch et al. (1991), have been cited as evidence that new axonal MT polymer arises by local assembly along the axon or at the growth cone during axon growth. More recently, a study using photoactivation approaches confirmed MT transport in embryonic *Xenopus* neurons but did not detect any movement in mouse dorsal root ganglion neurons (Okabe and Hirokawa, 1992).

In principle, the techniques of photoactivation and photobleaching should be capable of detecting the movement of tubulin regardless of the form in which it is moving. Thus, the significance of studies that have not demonstrated any directional movement of tubulin during axonal elongation is presently unclear, because tubulin must be actively transported along axons in some form to support sustained growth. Nevertheless, these studies have raised questions about the extent to which polymer transport contributes to the net addition of axonal MT polymer during axon growth. In fact, experiments using microinjection of haptenized tubulin have demonstrated that tubulin subunits can diffuse from the cell body into the neurite and assemble locally onto the ends of existing neuritic MTs (Okabe and Hirokawa,

1. *Abbreviations used in this paper*: CCD, charge-coupled device; MT, microtubule; tyr-tubulin, tyrosinated α-tubulin.

1988; Keith and Blane, 1990). In short neurites, such as those generally used for experiments in cell culture, it is possible that diffusion of tubulin subunits and local assembly onto the ends of existing MTs could contribute significantly to the increase in axonal MT mass during axon growth (p. 30 in Lasek, 1988; Black and Smith, 1988; Reinsch et al., 1991). One way to address the relative contribution of polymer transport and local assembly to the net addition of MT polymer to the growing axon is to identify the sites of MT formation in neurons. In this paper we present data that address this issue.

To identify potential sites for the formation of axonal MTs, we have investigated the distribution of young (newly assembled) MTs in neurons during axon growth. Newly assembled MTs were identified on the basis of their relative content of tyrosinated α-tubulin (tyr-tubulin). α-tubulin is synthesized with a tyrosine residue at its COOH terminus. This tyrosine residue can be removed posttranslationally by tubulin carboxypeptidase and then replaced by tubulin tyrosine ligase (reviewed in Barra et al., 1988; Bulinski and Gundersen, 1991). The substrate specificities of these enzymes are distinct. The tubulin carboxypeptidase acts on polymerized tubulin, whereas the tubulin tyrosine ligase acts on unassembled tubulin. Consequently, detyrosinated tubulin is found almost exclusively in polymer, and the number of detyrosinated tubulin subunits increases progressively with polymer age. Because the amount of detyrosinated tubulin in a polymer increases at the expense of the tyrosinated subunits, the relative content of tyr-tubulin in polymer varies inversely with MT age; recently assembled MTs contain higher amounts of tyr-tubulin than older, more long-lived MTs (Bré et al., 1987; Gundersen et al., 1987; Kreis, 1987; Schulze et al., 1987; Sherwin et al., 1987; Webster et al., 1987; Wehland and Weber, 1987; Sherwin and Gull, 1989).

In the present study we have combined fluorescence ratio imaging and a novel application of digital image processing and analysis techniques to analyze quantitatively spatial variations in the tyr-tubulin content of MTs in neurons. Using these methods, we demonstrate that MT polymer richest in tyr-tubulin is concentrated in two regions of growing neurons; one in the cell body, that extends into the proximal axon, and the other in the distal axon, that peaks in the growth cone. The relatively high content of tyr-tubulin among the MTs in these regions suggests that these regions are rich in newly assembled MTs in comparison with the axon shaft. A number of previous studies on MT dynamics in neurons have focused attention on the growth cone as the principal site of MT assembly during axon growth (reviewed in Hollenbeck, 1989). Our studies indicate that the proximal region of the neuron is also a major site of MT dynamics and thus also represents a potential site of MT formation for the growing axon.

Materials and Methods

Cell Culture

Cultures were grown on glass coverslips in 35-mm plastic tissue culture dishes. To prepare the culture dishes, a hole (10 mm in diameter) was drilled through the bottom of each dish (Nunc, DK-4000, Roskilde, Denmark) and then an acid-washed glass coverslip (22 × 22 mm, No. 1 thickness) was placed under the hole and fixed in place using a 3:1 mixture of paraffin and vaseline. The coverslips were coated with poly-D-lysine (70–150 kD) (Sigma Chemical Co., St. Louis, MO) and then laminin (Collaborative Research Inc., Bedford, MA, or Sigma Chemical Co.) essentially as described by Higgins et al. (1991).

Sympathetic neurons were dissociated from superior cervical ganglia of neonatal rat pups (CD strain, Charles River, Wilmington, MA) as described previously (Black and Kurdyla, 1983) and then plated on to poly-lysine/laminin-coated coverslips in serum-free medium essentially as described by Higgins et al. (1991). The medium contained a 1:1 mixture of Ham's F-12 (Gibco Laboratories Life Technologies, Inc., Grand Island, NY) and DME (Gibco Laboratories), supplemented with 0.5 mg/ml BSA (Fraction V, Calbiochem Corp., La Jolla, CA), 0.1 mg/ml bovine transferrin, 10 μg/ml bovine insulin, 5 ng/ml sodium selenite, 0.2 mg/ml L-glutamine (all from Sigma Chemical Co.), and 50 ng/ml nerve growth factor. Nerve growth factor was purified from mouse salivary glands by the method of Mobley et al. (1976). Cultures were maintained in an incubator at 37°C with a controlled atmosphere of 5% CO_2 and 95% humidity.

All the studies presented here were performed on cultures that varied between 17 and 21 h in age from the time of plating. By this time, most cells had extended one or more long slender axons (average = 2 axons per cell) and no dendrites (see also Bruckenstein and Higgins, 1988*a*,*b*). The axons had a mean length of ~0.4 mm and exhibited minimal branching or fasciculation. The simple and planar morphology of these neurons make them particularly suitable for quantitative image analysis.

Extraction of Unassembled Tubulin

Before immunostaining, the neurons were permeabilized with nonionic detergent under conditions that stabilize existing MTs to extract unassembled tubulin (see Results). Cells were rinsed once with PBS, once with PHEM (60 mM Pipes, 25 mM Hepes, 10 mM EGTA, 2 mM $MgCl_2$, pH 6.9) (Schliwa and van Blerkom, 1981), and then extracted for 5 min in PHEM containing 1% saponin (Sigma Chemical Co., prepared from Gypsophila sp.), 10 μM taxol (a gift from Dr. Mathew Suffness of the National Cancer Institute) and 0.1% DMSO (Sigma Chemical Co.). In some experiments, the extraction solution also contained a mixture of protease inhibitors (0.2 trypsin inhibitory units per 1 ml of aprotinin, and 10 μg/ml each of leupeptin, chymostatin, and antipain), but this had no apparent effect on the staining patterns for β-tubulin and tyr-tubulin. In some experiments, the cells were permeabilized in the presence of calcium to depolymerize the MTs. For these experiments, the extraction solution consisted of 60 mM Pipes, 25 mM Hepes, 1 mM $CaCl_2$, 2 mM $MgCl_2$, pH 6.9 (PHCM), and contained 1% saponin and no taxol.

Immunofluorescence

After extraction of the unassembled tubulin from the cells, the neuronal MTs were fixed and stained by one of two protocols.

Protocol 1. Extracted cultures were immersed in methanol (A.C.S. grade, Aldrich Chemical Co., Milwaukee, WI) at −20°C for 6 min, rehydrated by rinsing in PBS, treated with blocking solution (4% normal goat serum in PBS) for 10 min at room temperature, and then incubated with the primary antibody mixture for 45 min at 37°C. After this incubation, the cultures were rinsed thoroughly with PBS, treated with blocking solution as above, and then incubated with the secondary antibody mixture for 45 min at 37°C. The cultures were then rinsed with PBS and mounted in an aqueous solution containing 50% glycerol and 10 mg/ml n-propyl gallate (Sigma Chemical Co.). The primary antibody mixture contained a 1:100 dilution of a rat mAb specific for tyr-tubulin (YL1/2, Accurate Chemical and Scientific Corporation, Westbury, NY) (Kilmartin et al., 1982; Wehland and Willingham, 1983; Wehland et al., 1983) and a 1:750 dilution of a mouse mAb specific for β-tubulin (Amersham Corporation, Arlington Heights, IL) (Blose et al., 1984). The secondary antibody mixture contained a 1:100 dilution of FITC-conjugated goat anti-rat antibody and a 1:500 dilution of Texas red-conjugated goat anti-mouse antibody. Both secondary antibodies were purchased from Jackson Immunoresearch (Affini-Pure grade, preadsorbed for minimum cross-reactivity). All antibodies were diluted in blocking solution and then clarified immediately before use by centrifugation at 200,000 *g* for 10 min in a Beckman TL-100 ultracentrifuge (Beckman Instruments Inc., Palo Alto, CA).

Protocol 2. Extracted cultures were fixed for 10 min at room temperature by incubation in 2% (wt/vol) paraformaldehyde (BDH Chemicals Ltd., Poole, England) and 0.05% (wt/vol) glutaraldehyde (EM grade, Polysciences, Warrington, PA) in PHEM. The dishes were then rinsed with PBS and treated with 0.1% Triton X-100 (Sigma Chemical Co.) in PBS for 15 min. Subsequently, the dishes were rinsed with PBS, treated with three

5-min changes of sodium borohydride (10 mg/ml in a 1:1 mixture of PBS and methanol), and then rinsed with PBS again. Cultures were then processed for immunofluorescence as described for Protocol 1, except that the mAb against β-tubulin was used at a dilution of 1:200, and the Texas red-conjugated goat anti-mouse antibody was used at a dilution of 1:400.

Cells that were fixed according to *Protocol 1* and then processed without primary antibody exhibited very weak fluorescence, indicating that there was very little nonspecific binding of the secondary antibody. Cells that were fixed according to *Protocol 2* and then processed without primary antibody were noticeably brighter due to residual autofluorescence of aldehyde reaction products that were not reduced by the borohydride treatment (Osborn and Weber, 1982). To determine the contribution of this nonspecific fluorescence to our measurements, cells processed with or without first antibody using *Protocol 2* were imaged with a cooled charge-coupled device (CCD) camera using a constant exposure time, and the maximum fluorescence intensity of each cell body was determined. The average maximum fluorescent intensity for cell bodies processed without first antibody (n = 25 cells) was 3% of that for cell bodies stained with first antibody (n = 24 cells).

Image Acquisition

Cells were observed by differential interference contrast (DIC) and epifluorescence microscopy using a Zeiss Axiovert 35 inverted microscope (Carl Zeiss, Inc., Thornwood, NY). For epifluorescence microscopy, the cells were illuminated with a 100 W mercury arc lamp and observed using fluorescein (Zeiss filter set no. 10) and rhodamine (Zeiss filter set no. 14) filter sets. A heat-absorbing colored glass filter (BG40) was inserted into the light path between the light source and the filter block. For 35-mm photography, cells were photographed using TMAX 400 film (pushed to 800 ASA in the development) (Eastman Kodak Co., Rochester, NY). For quantitative analyses, images were captured using a CH250 cooled CCD camera (Photometrics Ltd., Tucson, AZ) that contained a Thompson 7883 CCD chip with a readout rate of 500 kHz. The temperature of the chip was maintained at ~−44°C. Image acquisition was performed on an Apple Macintosh IIfx computer using a Nu200 camera controller board and the BDS-Image image processing and analysis software package (Biological Detection Systems, Pittsburgh, PA). Illumination of the sample was controlled using a Uniblitz® electronic shutter (Vincent Associates, Rochester, NY), which was operated automatically from the BDS-Image software using a MAC 2000 Communications Interface Module (Ludl Electronic Products Ltd., Hawthorne, NY).

Images for analysis were acquired using the full usable area of the CCD chip, which measured 384 × 576 pixels, and stored in full 12-bit format on 650 megabyte magneto-optical disks using a Pinnacle REO-650 removable erasable optical disk drive (Pinnacle Micro Inc., Irvine, CA). Before capturing a series of images, an instantaneous readout of the bias voltage offset on the chip (the bias image) was saved and subsequently subtracted from each exposed image. Dark current (0.133 analog-to-digital units per second) was not significant for the exposure times used in these studies. The magnification of the CCD images was calibrated using a stage micrometer. Image processing and analysis was performed using the BDS-Image software and application programs written in this laboratory using the BDS-Image programming language. For maximum precision, all measurements of fluorescence intensity were performed on the 12-bit images. For presentation, images were scaled to 8-bits for display and photographed from the computer screen using a 35-mm camera equipped with a macro lens. Color images were photographed using Ektachrome 200 daylight film or Ektar 125 film and black and white images were photographed using TMAX 100 film (Eastman Kodak Co.).

Image Registration

Standard filter sets for fluorescence microscopy introduce a positional shift in the images that causes images viewed with different filter sets to be slightly out of register. This is primarily a consequence of lack of planarity of the barrier filters (Miller, 1991). Images acquired with the CCD camera using the standard Zeiss filter sets were approximately two pixels out of register with each other, which corresponded to a distance of ~0.45 μm using a 100× objective and ~1.7 μm using a 25× objective. Images were registered to within half a pixel by shifting each fluorescein image horizontally and vertically to achieve maximum overlap with the corresponding Texas red image. In later experiments the barrier filters in the standard filter sets were replaced with improved ultra-flat dielectric multilayer barrier filters obtained from Carl Zeiss Inc. Images that were captured using these filters were in register to within half a pixel in both the horizontal and vertical dimensions and did not require further registration in either direction.

Ratio Imaging

All images for ratio imaging were captured using the improved ultra-flat barrier filters from Carl Zeiss Inc. (see above) and a 100×/1.3 NA Plan-neofluar oil-immersion objective. The raw images of the fluorescein and Texas red fluorescence were corrected for nonuniformities in the illumination by flat-field correction and then corrected for the intensity of the background by background subtraction. To obtain flat-field images for flat-field correction, the specimen was removed from the light path and an image was acquired for both the rhodamine and fluorescein filter sets. To perform the flat-field correction, each pixel in the image to be corrected was divided by the corresponding pixel in the flat-field image for that fluorochrome. The resulting image was then multiplied by the average value of the pixels in the entire flat-field image. After flat-field correction, a histogram of the background pixel intensities in the image yielded a narrow and symmetrical bell-shaped curve, which is indicative of a uniform background. Background subtraction was performed by subtracting the mean background pixel intensity from each pixel in the flat-field corrected image and then setting any negative pixel values to zero.

To obtain a pixel-by-pixel ratio image, each pixel in the corrected image of the tyr-tubulin fluorescence was divided by the corresponding pixel in the corrected image of the β-tubulin fluorescence. The resulting ratio images were displayed using a pseudocolor map in which the magnitude of the ratio for each pixel was represented by the color hue and the amount of tubulin was represented by the color intensity. The spectrum of hues varied from violet (lowest ratio) to red (highest ratio), as shown in Fig. 3 *C*. The intensity of each pixel in the pseudocolor image was calculated from the image of the β-tubulin fluorescence by a nonlinear scaling procedure in which the intensity of each pixel in the pseudocolor image was proportional to the square root of the β-tubulin fluorescence intensity for that pixel. Details of these procedures, which are similar to the color coding method described by Paddy et al. (1990), will be provided upon request.

Quantitative Analysis Using a Segmented Mask

For these analyses, images of the tyr-tubulin and β-tubulin fluorescence were acquired using a 25×/0.8 NA Plan-neofluar oil-immersion objective. At this magnification, axons as long as 0.6 mm could be imaged within a single field. To quantify fluorescence intensity along the length of the axon, we used image processing techniques to generate a segmented mask of the neuron based on the image of the β-tubulin fluorescence. Each segment in the segmented mask was then used to define an area of measurement in the original images. The procedures for creating the mask and for subsequent measurement of the original images have been incorporated into a single interactive application program written in the BDS-Image programming language. A brief synopsis of these procedures is presented below, but a more detailed description will be provided upon request.

First, a high frequency spatial filter was applied to the image of the β-tubulin fluorescence to accentuate the edges of the cell body and the axons without distorting their position. Then, a thresholding operation was performed on the filtered image, and extraneous objects were removed using an interactive editing routine. The result was a binary mask of the image that included only the cell body, axon, and growth cone of interest. At points where the axon branched, we generally edited the mask to remove the thinner of the two branches so that the mask followed the course of the thicker branch. The edited mask was expanded by one pixel in all directions, and then divided into contiguous 2.6-μm-long segments by performing a constrained distance transformation. An example of a segmented mask is shown in Fig. 4.

To quantify the fluorescence intensity along the axon, the segmented mask of the neuron was overlaid on the original image of the β-tubulin fluorescence and on the registered image of the tyr-tubulin fluorescence. This allowed us to define segments in the β-tubulin and tyr-tubulin images that corresponded to the segments in the mask. To correct for background fluorescence in each image, an average background pixel intensity was calculated for each segment and then subtracted from each pixel within that segment (details will be provided on request). Then, the total fluorescence intensity for each segment of the β-tubulin and tyr-tubulin images was calculated by summing the corrected intensities of the pixels within each segment. A fluorescence ratio was also computed for each segment by dividing the total intensity for each segment in the image of the tyr-tubulin fluorescence by the total intensity for the corresponding segment in the image of the β-tubulin fluorescence. The fluorescence intensities and ratios were

plotted against distance along the long axis of the neuron, beginning at the cell body and ending at the growth cone (see Fig. 5).

Evaluation of the Masking Procedure

To evaluate the efficacy of the masking procedure for defining the boundary of the neuron, we overlaid the mask of a neuron on the image of the β-tubulin fluorescence from which it was derived and measured the proportion of the cell fluorescence that was contained within the mask at different sites within the cell body and along the axon. At each site, we determined pixel intensities along a line drawn perpendicular to the long axis of the mask, and subtracted the background from each pixel value. A graph of the corrected pixel intensities versus distance along the line yielded a bell-shaped curve (see Fig. 1). The total fluorescence intensity was determined by summing the intensities of all the pixels under the curve, and the fluorescence intensity within the mask was determined by summing the intensities of only those pixels that lay within the boundaries of the mask. The average proportion of the cell fluorescence that was contained within the mask was 93 ± 7% (mean ± SD, minimum = 76%, maximum = 98%) for 15 different sites within the cell body and 98 ± 3% (mean ± SD, minimum = 89%, maximum = 100%) for 23 different sites along the axon. There was no consistent variation in this proportion along the length of the axon. Fig. 1 shows representative line profiles for four different sites along a single neuron. These observations demonstrate that the mask is a faithful representation of the boundaries of the neuron and that a large majority of the cellular fluorescence was contained within the mask boundaries at all sites along the neuron.

Results

Experimental Design

We have investigated the relative proportion of tyr-tubulin in MTs in different regions of cultured sympathetic neurons. Neurons were permeabilized under conditions that stabilize existing MTs to extract unassembled tubulin and then double-stained for tyr-tubulin and β-tubulin using immunofluorescence procedures. Under these conditions, the intensity of the fluorescence is a relative measure of the amount of tyr-tubulin and β-tubulin in MT polymer. We have used the amount of β-tubulin in MTs as a relative measure

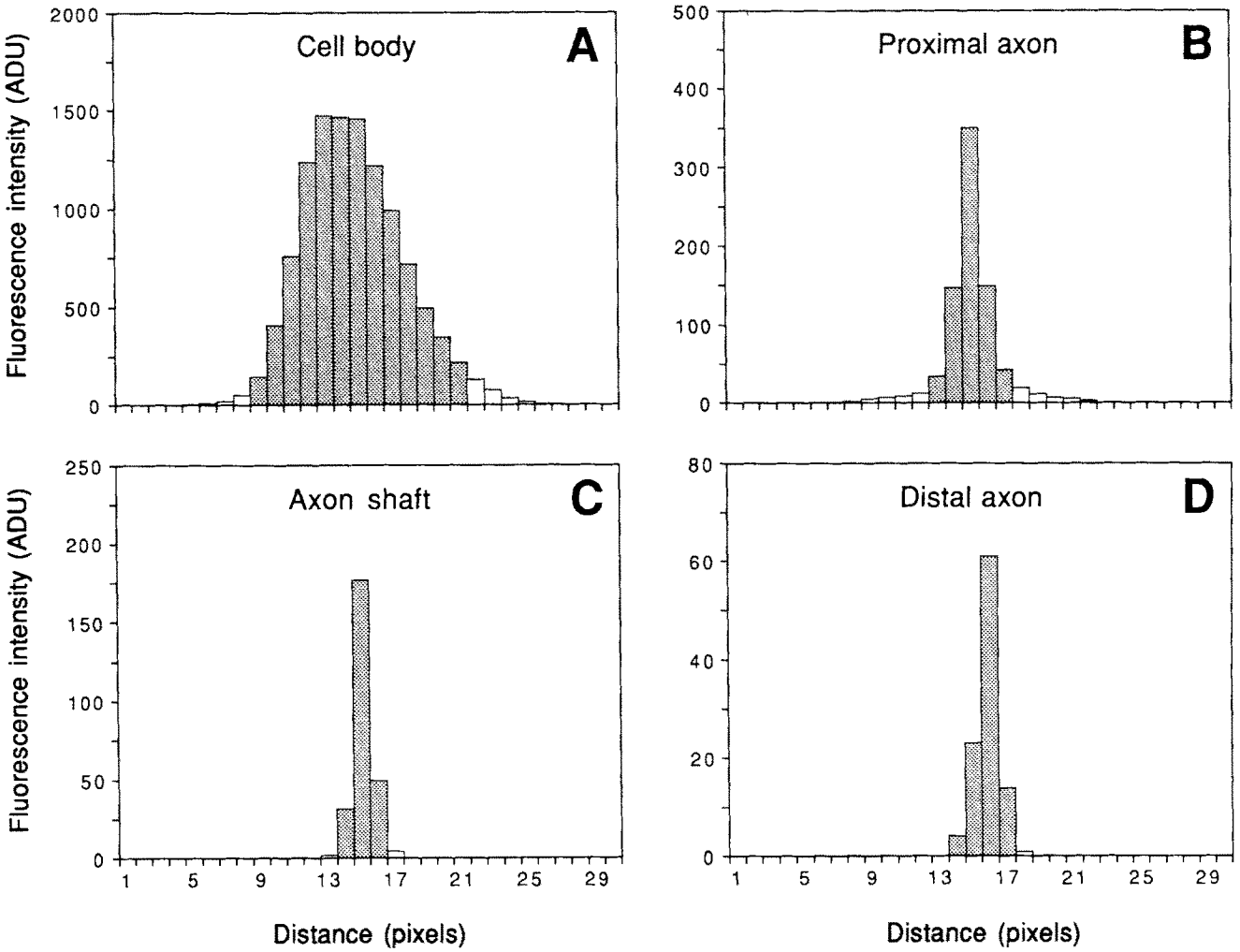

Figure 1. Evaluation of the masking procedure. Graphs showing the pixel intensity profiles for the β-tubulin fluorescence at four different sites along a single neuron. Each graph represents the pixel intensities along a line drawn perpendicular to the long axis of the neuron. (▨) Pixels that lie within the mask; and (□) pixels that lie outside the mask. These data were derived from the neuron shown in Fig. 4. *A* is a profile taken across the cell body, avoiding the nucleus, and *B* is a profile taken across the initial segment of the axon (see *arrow* in Fig. 4 *C*). *C* and *D* are profiles taken across the axon at distances of 217 (axon shaft) and 378 (distal axon) μm from the initial axon segment, respectively (total axon length = 399 μm). The proportion of the cell fluorescence that was contained within the mask was 97% in *A*, 90% in *B*, 98% in *C*, and 99% in *D*.

of polymer mass. This is valid because β-tubulin is present in a constant stoichiometry in MTs. In addition, the specific mAb to β-tubulin that we used recognizes all isotypes of β-tubulin (Joshi and Cleveland, 1989) and stains all MTs uniformly in the axons of rat sympathetic and other neurons (Joshi and Cleveland, 1989; Baas and Black, 1990). To quantify the fluorescence intensity due to tyr-tubulin and β-tubulin, we captured images of the cells using a cooled CCD camera and measured the fluorescence intensity in the cell body and along the axon using digital image processing and analysis techniques. Then, to determine the relative amount of tyr-tubulin in the MTs, we computed the ratio of tyr-tubulin fluorescence to β-tubulin fluorescence as a function of position in the neuron.

To extract unassembled tubulin under conditions that stabilize the existing MTs, we permeabilized neurons with 1% saponin in PHEM containing 10 μM taxol (see Materials and Methods). We have shown previously that MTs of cultured neurons are stabilized very effectively by permeabilization under these solution conditions and that there is negligible taxol-induced polymerization of soluble tubulin during the extraction (Black et al., 1986). It was important to remove the unassembled tubulin because most or all of this is tyrosinated (Gundersen et al., 1987), and thus its presence could lead to inaccuracies in our determination of the amounts of tyr-tubulin in MT polymer. To test the efficiency with which unassembled tubulin was extracted from the neurons, we permeabilized cells in the presence of 1 mM Ca^{2+}, which causes ≥92% of the MTs to depolymerize (Black et al., 1984), and then stained them for β-tubulin. If the extraction of unassembled tubulin from the permeabilized cells is effective, then cells permeabilized under these conditions should contain very little tubulin in comparison with cells extracted under conditions that stabilize MTs. We found that the cell bodies of neurons permeabilized under depolymerizing conditions showed only faint β-tubulin fluorescence and that the axons showed no detectable fluorescence (Fig. 2 *E*). In contrast, neurons permeabilized under conditions that stabilize MTs stained brightly for tubulin in both their cell bodies and their axons (Fig. 2, *A* and *C*). From these experiments, we conclude that our permeabilization conditions result in effective removal of unassembled tubulin, and therefore that the staining of cells permeabilized under MT-stabilizing conditions is due specifically to tubulin in MTs.

Observations on the Distribution of β-tubulin and Tyr-tubulin among Neuronal MTs

Fig. 2 shows photographs of neurons that were fixed with the aldehyde protocol (*A* and *B*) or with the methanol protocol (*C* and *D*), and then double-stained for β-tubulin and tyr-tubulin. Comparison of the β-tubulin fluorescence with images of the same cells taken using DIC optics indicated that MTs extended throughout the cytoplasm of the cell body and the axon (data not shown). At the distal end of the axon, the MT staining terminated at the base of the growth cone and sometimes the distal ends of the MTs were seen to splay apart slightly (for example, see Fig. 3, *D* and *E*). For 21 different axons, the average distance between the growth cone and the most distal extent of the MT staining was 2.2 ± 2.2 μm (mean ± SD, minimum = 0 μm, maximum = 7 μm).

All cells exhibited a characteristic pattern of staining for tyr-tubulin and β-tubulin that was independent of the method of fixation. Comparison of the staining patterns for tyr-tubulin and β-tubulin revealed both similarities and differences (Fig. 2 *A–D*). All regions of the neurons, except for the nucleus, stained for both tyr-tubulin and β-tubulin. In both cases the staining was considerably brighter in the cell body than in the axon. Moving out from the cell body into the proximal axon, the β-tubulin fluorescence declined over a distance of several tens of micrometers to reach a level that was relatively constant along the remainder of the axon shaft (Fig. 2, *A* and *C*). In contrast, the pattern of staining for tyr-tubulin within the axon was strikingly different (Fig. 2, *B* and *D*). Staining for tyr-tubulin was high in the proximal region of the axon, but declined to a much lower relative intensity within the axon shaft than was observed for β-tubulin. More distally, the staining for tyr-tubulin gradually increased again and appeared to reach another peak in the region of the growth cone (see also Baas and Black, 1990). These observations suggest that the relative proportion of tyr-tubulin in MTs is greater in the proximal and distal regions of the neuron than in the axon shaft. In the following sections, we present quantitative analyses of these staining patterns which confirm and extend this visual impression.

Visualization of the Relative Proportion of Tyr-tubulin among Neuronal MTs by Ratio Imaging

We used fluorescence ratio imaging to visualize the relative proportion of tyr-tubulin in MTs in different regions of the neuron. Fig. 3, *A–F* shows CCD images of the β-tubulin and tyr-tubulin fluorescence, and pseudocolor representations of the corresponding ratio images, for a cell body (Fig. 3, *A–C*) and for three growth cones (Fig. 3, *D–F*). The pseudocolor ratio images reveal unambiguously that the ratio is highest in the cell body and growth cone and lowest in the axon shaft. Moving out from the cell body into the proximal axon, the ratio declines gradually over several tens of micrometers to reach a constant low level within the axon shaft, and then gradually rises again more distally to reach a peak in the region of the growth cone. These observations confirm our visual impression that the MTs in the cell body and proximal axon and in the growth cone and distal axon contain a higher proportion of tyr-tubulin than MTs in the axon shaft.

In addition to these regional differences along the axon, ratio imaging also revealed regional differences in the tyr-tubulin content of MTs within the cell body (Fig. 3, *C*, *G* and *H*). Comparison of the ratio images of 39 different cells showed that no two cell bodies were exactly alike, but all of the neurons analyzed exhibited a similar general pattern in which the ratio was highest toward the periphery of the cell body and lowest toward the center. These observations indicate that MTs at the periphery of the cell body have a higher average proportion of tyr-tubulin than MTs toward the center of the cell body. However, in all cells the minimum ratio encountered in the cell body always exceeded the ratio in the axon shaft (for example, no violet or dark blue can be seen in the ratio images of the cell bodies in Fig. 3, *C*, *G*, and *H*).

Quantification of the Relative Proportion of Tyr-tubulin in MTs along the Axon

We have developed a novel approach that uses digital image processing and analysis techniques to quantify the relative proportion of tyr-tubulin among MTs in the cell body and

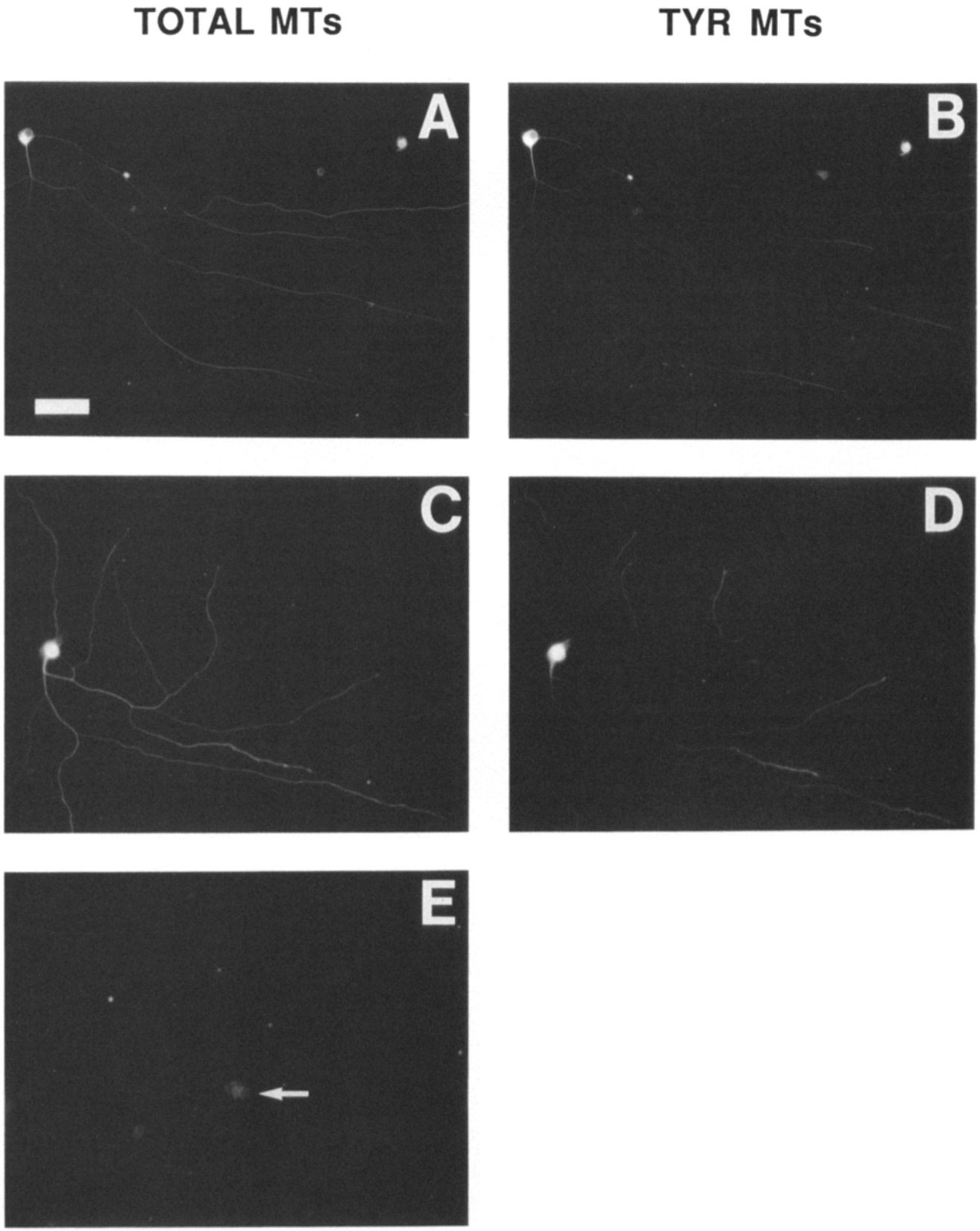

Figure 2. Visualization of β-tubulin and tyr-tubulin by immunofluorescence. Photographs of cells extracted under standard conditions that stabilize microtubules (PHEM + 1% saponin + taxol; *A–D*) and under modified conditions that depolymerize microtubules (PHCM + 1% saponin; *E*). The cell shown in *A* and *B* was fixed using the aldehyde fixation protocol and the cells shown in *C* and *D* and in *E* were fixed using the methanol fixation protocol (see Materials and Methods). The cells in *A–D* were double-stained for total tubulin in MTs using antibody to β-tubulin (*A* and *C*) and for tyrosinated tubulin in MTs using the YL1/2 antibody (*B* and *D*). The cell in *E* was stained for total tubulin in MTs using antibody to β-tubulin. The arrow in *E* indicates the position of the cell body. Note that the staining intensity of the neuron in *E* is negligible compared with the cells in *A* and *C*. Bar, 50 μm.

along the axon (see Materials and Methods). For each cell, a segmented mask was generated that faithfully defined the location of the cell body, axon, and growth cone of interest. Fig. 4 shows CCD images of the β-tubulin (Fig. 4 *A*) and tyr-tubulin (Fig. 4 *B*) fluorescence, and the corresponding segmented mask (Fig. 4 *C*), for a single representative neuron. In Fig. 4 *D*, the segmented mask (Fig. 4 *C*) is shown superimposed on the image of the β-tubulin fluorescence (Fig. 4 *A*), from which it was generated, to illustrate the close correspondence between the shape of the mask and the shape of the neuron (see Materials and Methods for a quantitative evaluation of the efficacy of the masking procedure).

To measure the relative distribution of β-tubulin and tyr-tubulin along the axon, the segmented mask was overlaid on the images of the β-tubulin and tyr-tubulin fluorescence. This allowed us to define segments in these images that corresponded to the segments in the mask. The intensities of the pixels within each segment of the β-tubulin and tyr-tubulin images were corrected for background and then summed to obtain a total fluorescence intensity for each segment in each image (see Materials and Methods). The fluorescence intensity within each segment of the tyr-tubulin image was then divided by the fluorescence intensity within the corresponding segment of the β-tubulin image to obtain a fluorescence ratio, which is a measure of the relative amount of tyr-tubulin in the MTs within that segment of the neuron. The fluorescence intensities for β-tubulin and tyr-tubulin in each segment and the corresponding ratio values were plotted against the distance along the long axis of the mask, measured from the cell body towards the growth cone (see Fig. 5).

We have analyzed 53 different cells using this method, 37 cells fixed with the methanol protocol and 16 cells fixed with the aldehyde protocol. The resulting intensity and ratio profiles for cells fixed by these two different methods were all similar in their overall shape, though each cell was unique in some way. Fig. 5, *A–C* show the results of the analyses for the cell shown in Fig. 4, and Fig. 5, *D–I* show the results of the analyses for two other cells. In all cells, the amount of tubulin within individual segments in the cell body was considerably greater than the amount of tubulin within individual segments in the axon (Fig. 5, *A*, *D*, and *G*). This reflects the fact that the cell body is considerably thicker and wider than the axon.

Within the axon, we frequently observed variations in the β-tubulin content of the segments. Since the amount of β-tubulin is a relative measure of the MT polymer mass, this indicates that the MT mass varied along the length of the axon. In many cases, the increase or decrease in MT mass appeared to correlate with a corresponding increase or decrease in axon caliber. Often these changes in caliber were associated with points at which the axon branched. For the 53 axons that we analyzed, there were a total of 123 branch points. In 50% of cases (62 out of 123), there was no clear difference in the MT mass within segments proximal and distal to a branch point (for example, see the middle branch point in Fig. 5 *H*), but in 27% of cases (33 out of 123) we observed a sharp decline in the MT mass distal to a branch (for example, see the most proximal branch in Fig. 5 *H*). In general, the magnitude of the decline in MT mass distal to a branch point appeared to reflect the degree of inequality between the caliber of the parent axon and the daughter branch. In 3% of cases (4 out of 123), the total tubulin content of the axon was observed to rise over a distance of many segments proximal to a branch (for example, see the most proximal and the most distal branch points in Fig. 5 *B*). This may reflect an accumulation of MTs due to a local impediment in their movement, such as has been described for axonally transported materials proximal to constrictions along axons (Weiss and Hiscoe, 1948; LeBeau et al., 1988)).

Fig. 5, *C*, *F*, and *I* show the fluorescence ratio profiles for three different cells. The magnitude of the fluorescence ratio is a measure of the relative amount of tyr-tubulin in the MTs (see above). In all neurons, the fluorescence ratio was high in the cell body and declined in the proximal region of the axon to reach a constant low level within the axon shaft. More distally, the ratio rose again to reach a peak at the distal end of the axon. Similar results were also obtained in a limited number of experiments in which the neurons were extracted in the presence of 0.4 M NaCl to remove MT-associated proteins from the MTs (Vallee, 1982). These results demonstrate quantitatively that MTs in the cell body and proximal axon and in the distal axon and growth cone contain a greater average proportion of tyr-tubulin than MTs in the axon shaft.

Within the axon, branch points and local variations in the MT mass had little or no effect on the proportion of tyr-tubulin in the MTs. For example, Fig. 5 *H* shows an abrupt decline in the MT mass along the axon at the most proximal branch point, but Fig. 5 *I* shows no clear change in the fluorescent ratio. Within the cell body, the fluorescence ratio was typically highest in the first and last segments, which contained only peripheral regions of the cell body, and lowest in the more central segments, which included the center of the cell body (for example, compare the ratio profile in Fig. 5 *C* with the corresponding segmented mask in Fig. 4 *C*). Thus, the ratio profile for the cell body reinforces the observations that we made using ratio imaging, which indicated that the average proportion of tyr-tubulin in MTs was generally greatest toward the periphery of the cell and lowest at its center (Fig. 3, *C*, *G*, and *H*). However, in spite of this spatial variation in the fluorescence ratio within the cell body, even the minimum segment ratio for the cell body was still greater than the segment ratios within the axon shaft, and this was true for all the cells that we analyzed.

To extract more detailed information from the ratio profiles, we subdivided them into four regions as illustrated in the schematic diagram in Fig. 6. This schematic is based on the average measurements for 53 different neurons (average axon length = 358 μm), and these measurements are summarized in Table I. While considerable variation existed between different cells, the following general observations applied to all cells: (*a*) In all cases, the segment ratios in the cell body and at the growth cone were higher than the segment ratios in the axon shaft; (*b*) on average, the maximum segment ratios in the cell body and at the growth cone were ~8- and 12-fold greater than the segment ratios in the axon shaft, respectively; (*c*) the high ratio in the cell body extended into the proximal axon for all neurons, declining gradually over an average distance of 40 μm to reach a constant low ratio within the axon shaft; and (*d*) the ratio increased progressively in the distal region of the axon over an average distance of 110 μm, reaching a maximum value in the region of the growth cone. In all cases the maximum ratio in the distal region of the axon was located within a few mi-

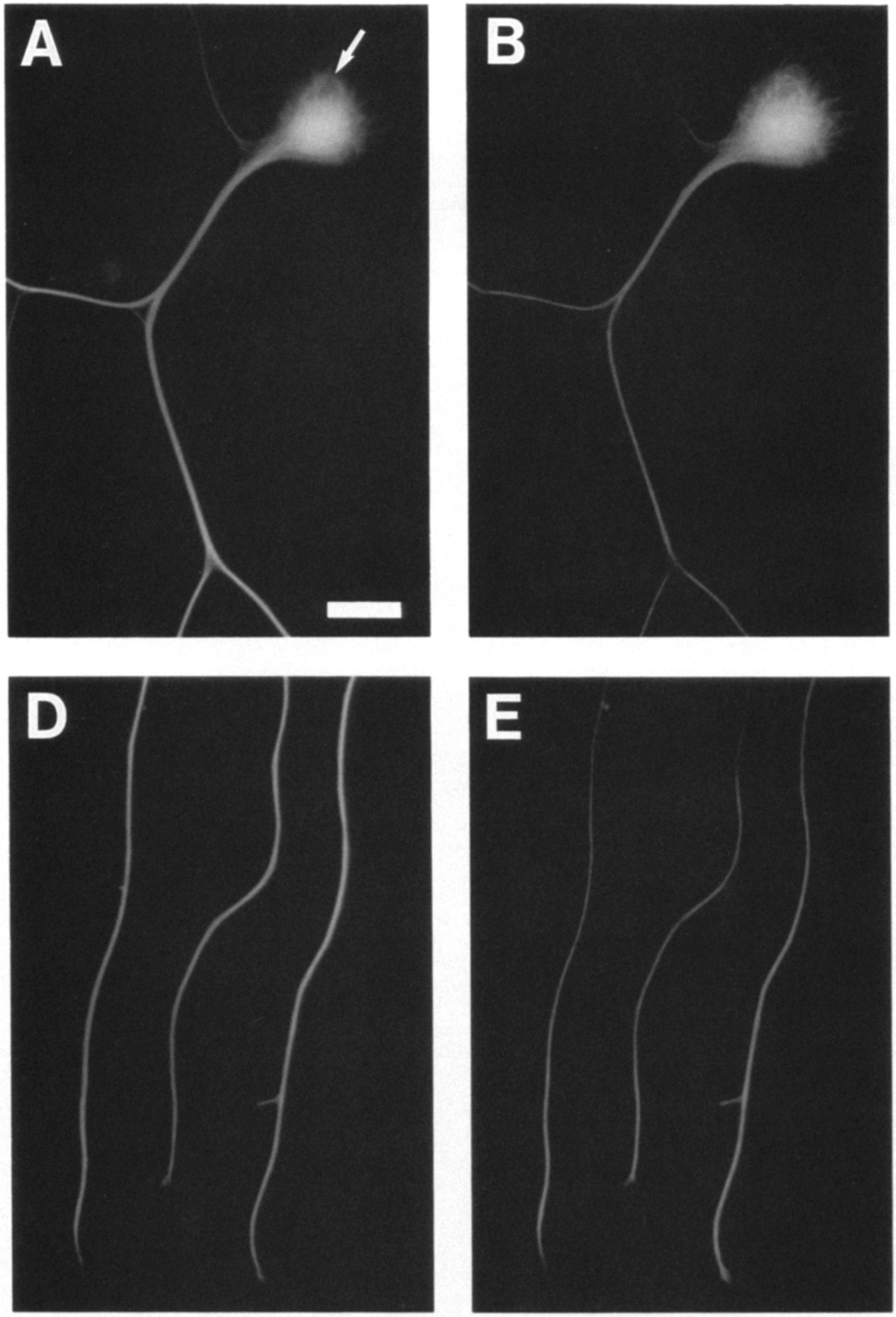

Figure 3. Ratio imaging of the cell body and growth cone. *A* and *B* show CCD images of a cell body and the proximal region of its two axons; the outline of the nucleus is indicated by the arrow in *A*. *C* shows a pseudocolor representation of a ratio image obtained by dividing the image shown in *B* by that shown in *A*. *D* and *E* show CCD images of the growth cones and distal regions of three axons; at the growth cone, the MTs can be seen to splay apart slightly. *F* shows a pseudocolor representation of a ratio image obtained by dividing the image shown in *E* by that shown in *D*. *G* and *H* are the pseudocolor ratio images for two other cell bodies. All of these cells were fixed using the aldehyde fixation protocol, but similar staining patterns were observed for cells that were fixed with methanol (data not shown). Similar

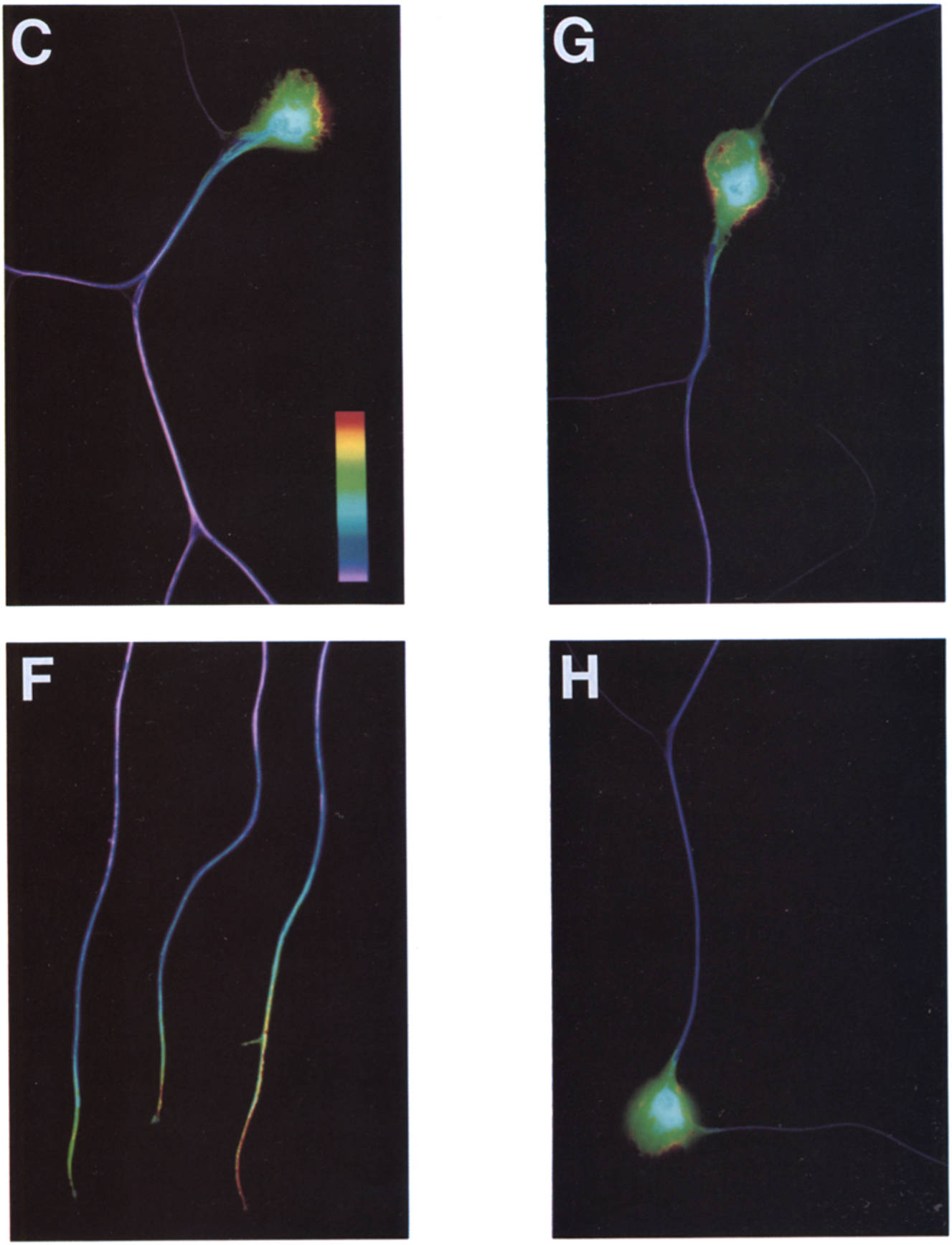

ratio images were also obtained for cells that were extracted with Triton X-100 (0.2%) instead of saponin (data not shown). The color key in *C* indicates the spectrum of colors used to represent the magnitude of the ratio. High ratios are represented by the color red and low ratios are represented by the color violet. Note the "hot spot" of high ratio overlying the nucleus in *G*, in which several filamentous structures rich in tyr-tubulin appear to extend from a discrete site. This could represent individual MTs extending from a microtubule nucleating structure within the soma. Bar, 15 μm.

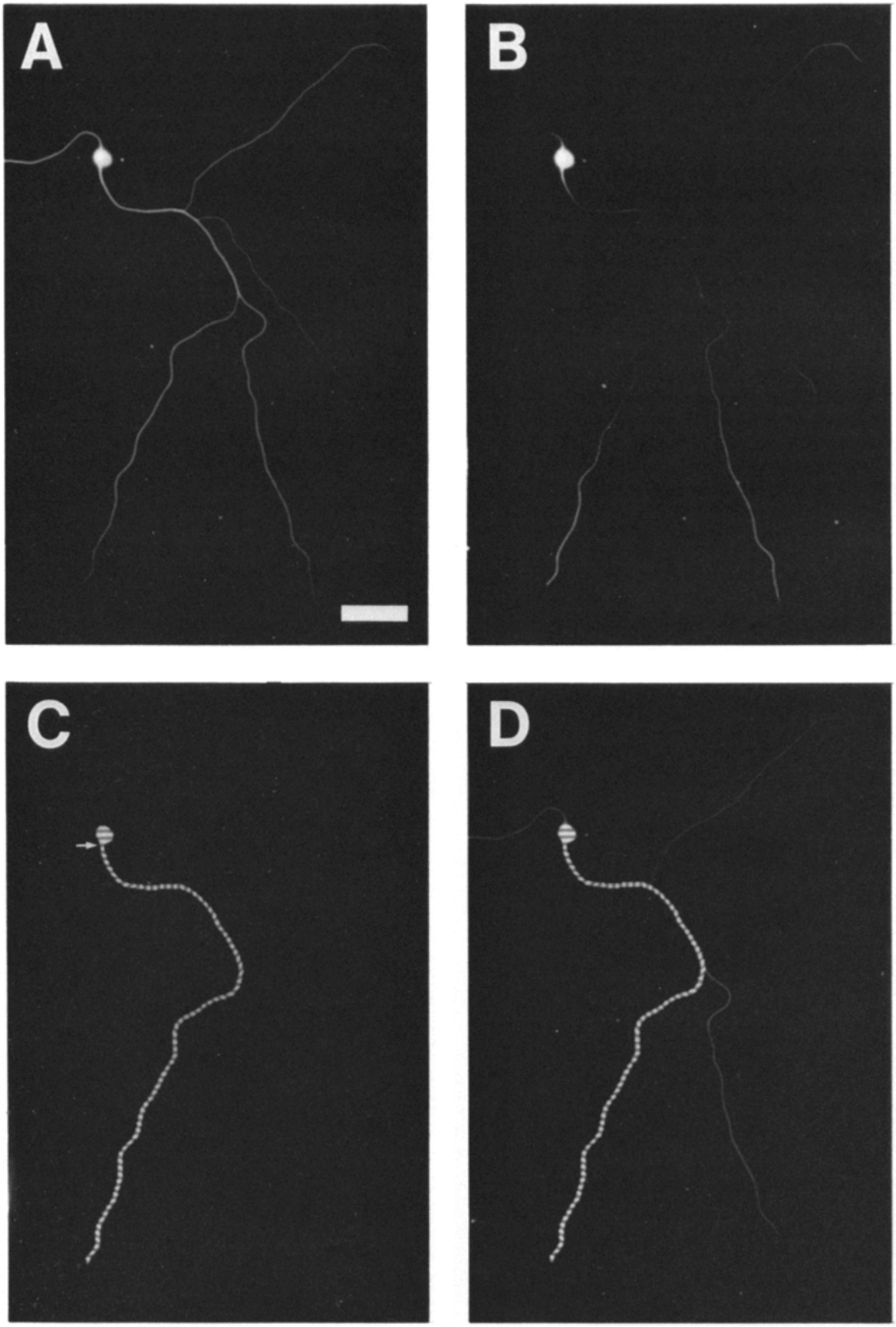

Figure 4. Segmentation of a neuron for quantitative analysis. CCD images of a neuron that was double-stained for β-tubulin (*A*) and tyr-tubulin (*B*). *C* shows an image of the corresponding segmented mask for this neuron and *D* shows the same mask superimposed on

crometers of the growth cone (average = 3 μm, minimum = 0 μm, maximum = 19 μm, n = 53).

It is important to note that the ratio value obtained for each segment in these quantitative analyses represents an average tyr-tubulin content for all of the MT polymer contained within that segment. Our ratio imaging studies revealed that there are marked spatial variations in the tyr-tubulin content of MTs within the cell body (see Fig. 3, *C*, *G*, and *H*) and this heterogeneity exists within each individual segment of the cell body defined by the segmentation procedure (for example, compare the segmented mask in Fig. 4 with the ratio images of the cell bodies in Fig. 3). Therefore, quantitative analyses using the segmented mask procedure are likely to underestimate the magnitude of the maximum ratio for the cell body. In contrast, the segmentation analyses are likely to be a more reliable estimate of the maximum ratio for the growth cone since ratio imaging of distal axons did not reveal spatial variations comparable with those in the cell body (Fig. 3 *F*). In any event, the data show unequivocally that the average proportion of tyr-tubulin in MTs is considerably greater in the cell body and at the growth cone than in the axon shaft.

Fig. 7 shows scatter plots of the lengths of Region B (proximal axon), Region C (axon shaft) and Region D (distal axon) plotted against axon length. The lengths of the axons ranged from 161 to 569 μm and there was considerable variation in the lengths of the three regions in different axons. Statistical analysis revealed a strong positive correlation between the lengths of Region C (axon shaft) and axon length ($p < 0.001$), but a weaker correlation for Region B (proximal axon, $0.05 < p < 0.1$) and Region D (distal axon, $0.01 < p < 0.02$). However, the most striking feature of these plots is that the length of Region C shows a much greater increase with increasing axon length than for Regions B and D. This indicates that the lengths of Regions B and D are less dependent on axon length than Region C and that the increase in axon length during axon growth is due principally to an increase in the length of Region C.

Discussion

We have applied digital image processing and analysis techniques to quantify the relative tyr-tubulin content of MTs in the cell bodies and along the axons of cultured sympathetic neurons. Neuronal cytoskeletons were double-stained with antibodies specific for β-tubulin and tyr-tubulin using immunofluorescence procedures and then imaged using a cooled CCD camera. The fluorescence intensities due to β-tubulin and tyr-tubulin were quantified in the cell body and along the axon. Then, the relative proportion of tyr-tubulin in MTs was determined by calculating the ratio of the tyr-tubulin fluorescence to the β-tubulin fluorescence as a function of position in the neuron using (*a*) conventional pixel-by-pixel ratio imaging, and (*b*) a procedure in which each neuron was subdivided into contiguous segments (the segmentation procedure). The segmentation procedure allowed us to quantitatively analyze the tyr-tubulin content of MTs along the length of individual axons and the computational applications that we have developed should be generally applicable to a wide range of studies on the regional differentiation of cytoskeletal polymers in neurons. In the present study, we have used these methods to demonstrate that the tyr-tubulin content of MTs varies with location in the neuron. These findings are discussed in terms of regional variations in MT age and MT assembly activity within the neuron.

MTs Rich in Tyr-tubulin Are Concentrated in the Proximal and Distal Regions of Growing Neurons

Ratio imaging provided a striking visual demonstration that the ratio of tyr-tubulin to β-tubulin varied as a function of location in the neuron (see Fig. 3) and the segmentation procedure allowed us to quantify these regional differences (see Figs. 4 and 5). Together, these analyses revealed two regions of the neuron in which the ratio was relatively high, one in the cell body and the other in the growth cone. Moving out from the cell body into the axon, the ratio declined over an average distance of 40 μm (Region *B* in Fig. 6) to reach a constant low value within the axon shaft (Region *C* in Fig. 6) and then rose again more distally, over an average distance of 110 μm (Region *D* in Fig. 6), to reach a second peak at the growth cone (see Table I). On average, the maximum segment ratios in the cell body and growth cone were ~10-fold higher than the segment ratios in the axon shaft (see Table I). In this discussion, we shall refer to the cell body and proximal axon (Regions *A* and *B* in Fig. 6) as the proximal region of the neuron, and to the distal axon and growth cone (Region *D* in Fig. 6) as the distal region of the neuron.

In both the ratio imaging and segmentation procedures, the ratio of the tyr-tubulin fluorescence to the β-tubulin fluorescence in each pixel or segment represents the average tyr-tubulin content for all the MT polymer within that region. Therefore, our observation of regional differences in the ratio of tyr-tubulin to β-tubulin in these neurons indicates that the average content of tyr-tubulin in the MTs varies as a function of position in the neuron. Specifically, MTs in the proximal and distal regions of the neuron contain a higher average proportion of tyr-tubulin than MTs in the axon shaft.

Recent observations on individual MTs in the distal regions of these axons support the above conclusion. Specifically, we have developed a novel preparation using these neurons in which the MTs in the axon shaft and distal axon splay apart from each other so that individual polymers can be visualized using standard immunofluorescence procedures (Brown, A., Y. Li, T. Slaughter, and M. Black, manuscript submitted for publication). When the MTs in these preparations are stained for tyr-tubulin, all of the MTs in the distal 30–50 μm of the axon stains more brightly than any of the MTs in the axon shaft. These observations confirm that the average tyr-tubulin content of the MTs is greater in the distal axon than in the axon shaft. Furthermore, they indicate that

the image of the β-tubulin fluorescence (*A*), from which it was derived. Odd-numbered segments in the mask are white, and even-numbered segments are grey. The position of the initial axon segment, which is the most proximal segment of the axon, is marked with an arrow in *C*. This cell was fixed using the aldehyde fixation protocol, and the results of the quantitative analysis for this cell are shown in Fig. 5, *A–C*. Bar, 50 μm.

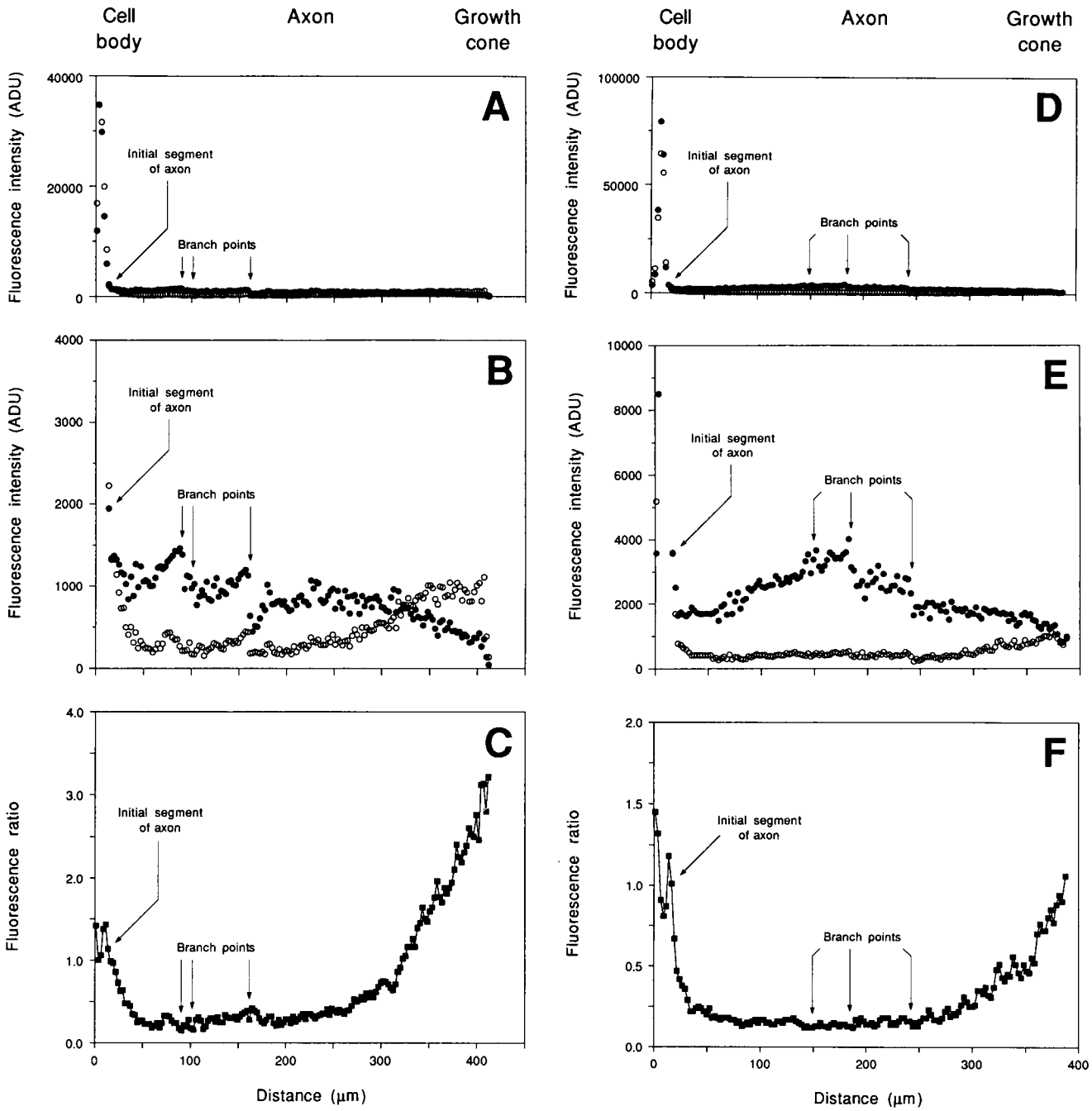

Figure 5. Results of the quantitative analysis for three neurons. The top graphs (*A*, *D*, and *G*) shows the distribution of tyr-tubulin (○) and β-tubulin (●) for each cell, the middle graphs (*B*, *E*, and *H*) show the same data plotted with a different scale on the ordinate to reveal details of the profile along the axon, and the lower graphs (*C*, *F*, and *I*) show the ratio of the tyr-tubulin fluorescence intensity to β-tubulin fluorescence intensity, which is a measure of the relative tyr-tubulin content of the MTs. All data are plotted against distance along the axis of the mask in μm, measured from the first segment in the cell body and extending towards the growth cone. Each point in the upper and middle graphs represents the fluorescence intensity for a single segment in the mask and each point in the lower graphs represents the fluorescence ratio for a single segment in the mask. The first and second cells (*A–F*) were fixed using the aldehyde fixation protocol, and the third cell (*G–I*) was fixed with methanol. The first cell (*A–C*) corresponds to the cell shown in Fig. 4. The position of the initial axon segment and any branch points along the axon are indicated on the profiles. Note that for each cell the absolute values of the intensities in upper and middle graphs are arbitrary analog-to-digital units (ADU) and thus the magnitude of the ratio in the lower graphs represents a relative measure of the proportion of tubulin that is tyrosinated.

the tyr-tubulin content of each of the MTs in the most distal region of the axon exceeds that of any of the MTs in the axon shaft. These preparations have not allowed us to visualize individual MTs in the cell bodies and proximal axons of these neurons, but it is likely that the high average tyr-tubulin content of the MTs in these regions also reflects a similar overall enrichment in tyr-tubulin of the individual MTs compared with the axon shaft. This is supported by immunoelectron microscopic studies in this laboratory which have shown that many more MT profiles stain densely for tyr-tubulin in the

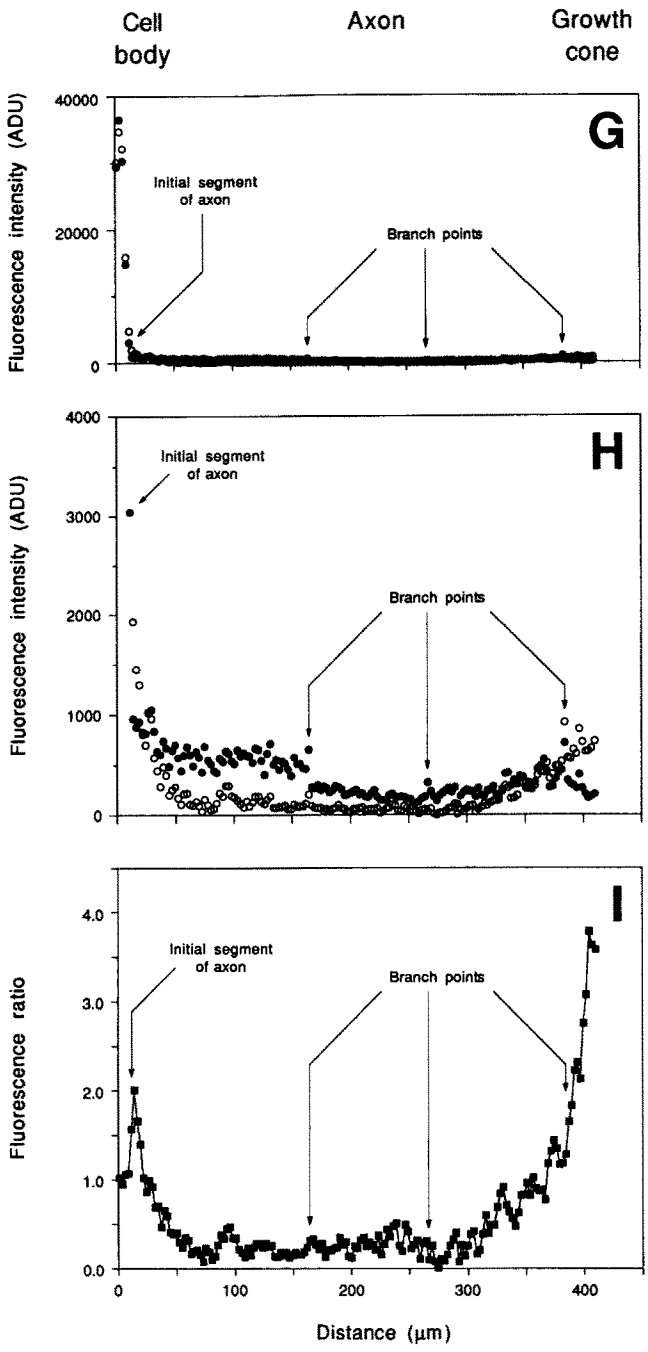

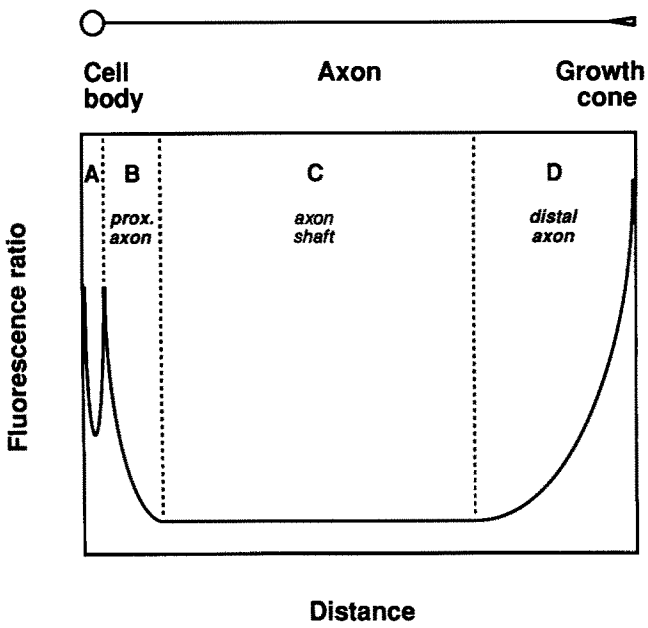

Figure 6. Schematic diagram of the variation in the fluorescence ratio along a typical axon. The relative dimensions of the ratio profile in this diagram are based exactly on the average dimensions for the 53 different cells that we have analyzed (see Table I). Each profile was subdivided into four regions: Region *A* (cell body) includes all segments proximal to the initial axon segment. Region *B* (proximal axon) includes the initial axon segment and extends distally to the point in the axon where the ratio declines to a constant level. Region *D* (distal region) extends from the point where the ratio starts to rise again to the distal end of the axon at the growth cone. Region *C* (axon shaft) lies between Regions *B* and *D*.

cell body and proximal axon, as well as in the distal axon, than in the axon shaft (Baas and Black, 1990; Baas et al., 1991; Baas, P., F. Ahmad, T. Pienkowski, A. Brown, and M. Black, manuscript submitted for publication). Collectively, these considerations indicate that MT polymer rich in tyr-tubulin is concentrated in the proximal and distal regions of these neurons.

Newly Assembled MTs Are Concentrated in the Proximal and Distal Regions of Growing Neurons

One interpretation for the regional variation in the tyr-tubulin content of MTs in these neurons derives from current understanding of the detyrosination of MTs in cells. Studies on several different cell types have revealed that detyrosination of α-tubulin occurs after polymerization and that the proportion of detyrosinated subunits in MTs increases with the age of the polymer (for example, see Kirschner and Mitchison, 1986; Sherwin and Gull, 1989; Bulinski and Gundersen, 1991; also see the introduction). Specifically, MTs that are newly assembled are rich in unmodified (tyrosinated) tubulin subunits and subsequently they gradually accumulate increasing numbers of modified (detyrosinated) tubulin subunits in a time-dependent manner. Thus, the proportion of tyr-tubulin in MTs varies inversely with the age of the polymer, with the highest proportion occurring in the most recently assembled polymer (Kirschner and Mitchison, 1986; Sherwin and Gull, 1989). On this basis, we suggest that the spatial variation in tyr-tubulin content of MTs in neurons reflects a corresponding variation in the age of these polymers. Thus, the youngest, most recently assembled MT polymer in the neuron is enriched in the proximal and distal regions compared with the axon shaft. This suggests that the proximal and distal regions of these neurons are especially active sites of MT assembly.

Our use of the tyr-tubulin content of MTs as a relative measure of MT age assumes that the tubulin carboxypeptidase activity is uniformly distributed throughout the neuron. The following observations support this assumption. First, immunofluorescence studies have demonstrated that MTs throughout the neuron stain with an antibody specific for detyrosinated α-tubulin (Gundersen and Bulinski, 1986; Lim et al., 1989; Baas et al., 1991, and our own unpublished data). In addition, immunoelectron microscopic analyses indicate that all MTs in the cell body, proximal axon, axon shaft, and

Table I. Summary of Ratio Profile Parameters

	Mean	Minimum	Maximum
Axon length	358 μm	161 μm	569 μm
Length of Region A (cell body)	15 μm	10 μm	23 μm
Length of Region B (proximal axon)	40 μm	18 μm	100 μm
Length of Region C (axon shaft)	208 μm	38 μm	419 μm
Length of Region D (distal axon)	110 μm	23 μm	235 μm
Max proximal ratio/mean axon ratio	8	2	24
Max distal ratio/mean axon ratio	11	3	25

These measurements are based on the analysis of the ratio profiles of 37 different cells from three different cultures fixed using the methanol protocol and 16 different cells from two different cultures fixed using the aldehyde protocol (total = 53 cells). The cultures varied in age from 17–21 h after plating. The mean number of axons per cell was 2 (minimum = 1, maximum = 4, n = 53), but only one axon was analyzed per cell. Axon length is defined as the distance from the most proximal segment of the axon (the initial axon segment) to the most distal segment of the axon, at the growth cone. Regions A–D are defined in the schematic diagram in Fig. 6. The maximum proximal ratio is the maximum ratio for the segments in Regions A and B (the cell body and proximal axon). The mean ratio in the axon was obtained by averaging the ratio values for all the segments in Region C (axon shaft). The maximum distal ratio is the maximum ratio for the segments in Region D (distal axon).

distal axon contain detectable amounts of detyrosinated α-tubulin (Baas et al., 1991). Second, when neurons are treated with taxol to stabilize their MTs, the tyr-tubulin content of the MTs decreases throughout the neuron (Robson and Burgoyne, 1989; Arregui et al., 1991; Mansfield and Gordon-Weeks, 1991). We have performed similar experiments on cultured sympathetic neurons, and have obtained comparable results. Specifically, we observed a time-dependent decrease in the tyr-tubulin content of MTs in the cell body and all regions of the axon (our unpublished data). These observations indicate that the tubulin carboxypeptidase is present and active throughout the neuron and this supports the above interpretation that the regional variation in the tyr-tubulin content of the MTs in these neurons reflects a corresponding regional variation in the age of these MTs.

The location of the sites of assembly of axonal MTs is an issue of long-standing interest and controversy in the cell biology of axon growth. A variety of different approaches have been used to address this issue, including microinjection of haptenized tubulin (Okabe and Hirokawa, 1988; Keith and Blane, 1990), microinjection of fluorescent tubulin followed by photobleaching (Lim et al., 1989, 1990; Okabe and Hirokawa, 1990), microinjection of caged fluorescent tubulin followed by photoactivation (Reinsch et al., 1991; Okabe and Hirokawa, 1992), and pharmacologic experiments using agents that perturb MT assembly dynamics (Bamburg et al., 1986). A number of these studies have focused attention on the growth cone as the principal site of MT assembly for the axon (reviewed in Hollenbeck, 1989; Nixon, 1992). While our studies confirm that the growth cone and distal axon are active sites of MT assembly in these neurons, they indicate that the cell body and the proximal axon are also active sites of MT assembly. This finding is consistent with the observations of Lim et al. (1989) on the recovery of fluorescence after photobleaching in the cell bodies and neurites of PC12 cells, and also with the observations of Arregui et al. (1991) on the recovery of MT staining for tyr-tubulin in cerebellar macroneurons after treatment with nocodazole. In fact, if the amount of tyr-tubulin in polymer is taken as a rough approximation of the amount of newly assembled polymer, then our data indicate that the amount of newly assembled polymer in the cell body exceeds that anywhere else in the neuron and greatly exceeds that in the distal axon, and that the amount of newly assembled polymer in the proximal 10–20 μm of the axon is at least equivalent to that in the distal 10–20 μm of the axon (see Fig. 5, *B*, *E*, and *H*). Collectively, these observations indicate that, in addition to the distal axon and growth cone, the cell body and proximal axon also represent potential sites for the formation of new axonal MT polymer in neurons during axon growth, and that these regions actually have the potential to generate more polymer for the axon than the distal axon and growth cone.

The relatively high levels of newly assembled MT polymer in the proximal and distal regions of neurons during axon growth may be due to dynamic turnover of MTs, to net assembly of new MT polymer, or to a combination of the two. For example, newly assembled MTs can be highly dynamic structures and may undergo repeated cycles of assembly and disassembly without any net increase in the total polymer mass (Mitchison and Kirschner, 1984). In this situation, which is typical of many cell types in culture (for example, see Soltys and Borisy, 1985; Schultze and Kirschner, 1986), many newly assembled MTs exist at any moment in time but there is no net addition of MT polymer. Alternatively, if the amount of assembly exceeds the amount of disassembly for the MT population, then the presence of newly assembled MTs will reflect the net addition of polymer. The present data do not permit us to evaluate the relative contribution of net addition and turnover to the newly assembled polymer in the proximal and distal regions of these neurons. However we have begun to address this question in a related study by investigating the sites of stabilization of MTs in neurons during axon growth (Baas, P., F. Ahmad, T. Pienkowski, A. Brown, and M. Black, manuscript in preparation). Most cells contain stable MTs, and in neurons, these relatively long-lived polymers are quite abundant (Brady et al., 1984; Ferreira et al., 1989; Baas and Black, 1990). Stable MTs appear early in neuronal development, and their levels increase progressively as the axon elongates (Ferreira et al., 1989; Arregui et al., 1991). We have found that the generation of stable MT polymer occurs to a much greater extent proximally, in the cell body and proximal axon, compared with the axon shaft and the distal axon. This suggests that the cell body and proximal axon are the principal sites of formation of new long-

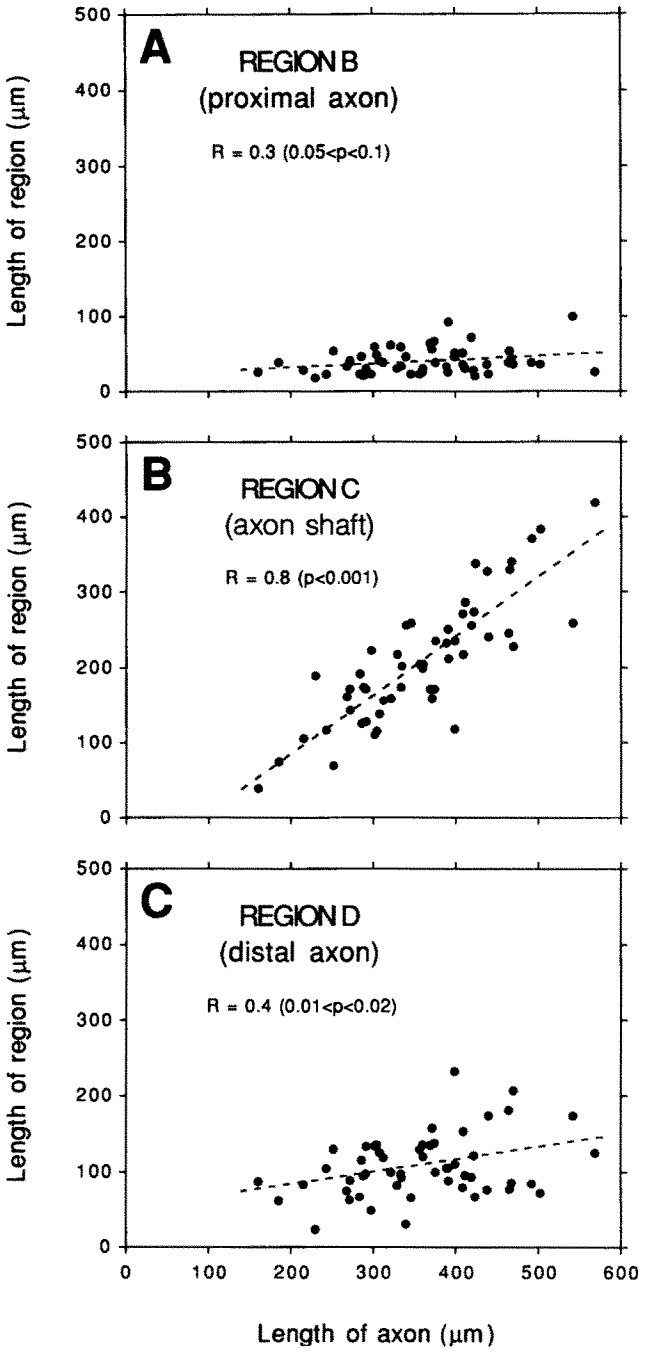

Figure 7. Dependence of the lengths of Regions B, C, and D on axon length. Scatter plots of the lengths of (*A*) Region B (proximal axon), (*B*) Region C (axon shaft), and (*C*) Region D (distal axon) plotted against axon length for 53 different axons (see Table I). Pearson's product-moment correlation statistic (R) is shown for each plot. A two-tailed t test was used to test the statistical significance of each correlation coefficient with respect to the null hypothesis that the data represented a sample from a population with no correlation between region length and axon length.

lived polymer for the growing axon and therefore that the high levels of polymer assembly that occur proximally contribute to the net addition of polymer to the axon.

This paper is dedicated to Wendy.

We thank Dennis Higgins for his helpful advice on culturing sympathetic neurons, Dave Patek and Cliff Glier of Biological Detection Systems Inc. for their assistance with the development of the image analysis programs, and Woollcot Smith for his advice on statistical matters.

This work was supported by a grant from the National Institutes of Health to M. M. Black.

Received for publication 9 June 1992 and in revised form 23 July 1992.

References

Arregui, C., J. Busciglio, A. Caceres, and H. S. Barra. 1991. Tyrosinated and detyrosinated microtubules in axonal processes of cerebellar macroneurons grown in culture. *J. Neurosci. Res.* 28:171–181.

Baas, P. W., and M. M. Black. 1990. Individual microtubules in the axon consist of domains that differ in both composition and stability. *J. Cell Biol.* 111:495–509.

Baas, P. W., T. Slaughter, A. Brown, and M. M. Black. 1991. Microtubule dynamics in axons and dendrites. *J. Neurosci. Res.* 30:134–153.

Bamburg, J. R., D. Bray, and K. Chapman. 1986. Assembly of microtubules at the tip of growing axons. *Nature (Lond.).* 321:788–790.

Barra, H. S., C. A. Arce, and C. E. Argaraña. 1988. Post-translational tyrosination/detyrosination of tubulin. *Mol. Neurobiol.* 2:133–153.

Black, M. M., and J. T. Kurdyla. 1983. Microtubule-associated proteins of neurons. *J. Cell Biol.* 97:1020–1028.

Black, M. M., and W. Smith. 1988. Regional differentiation of the neuronal cytoskeleton with an appendix: diffusion of proteins in the neuron cell body-mathematical approximations and computer simulations. *In* Intrinsic Determinants of Neuronal Form and Function. R. J. Lasek and M. M. Black, editors. Alan R. Liss, Inc., New York. 463–486.

Black, M. M., J. M. Cochran, and J. T. Kurdyla. 1984. Solubility properties of neuronal tubulin: evidence for labile and stable microtubules. *Brain Res.* 295:255–263.

Black, M. M., J. M. Aletta, and L. A. Greene. 1986. Regulation of microtubule composition and stability during nerve growth factor-promoted neurite outgrowth. *J. Cell Biol.* 103:545–557.

Blose, S. H., D. I. Meltzer, and J. R. Feramisco. 1984. 10 nm filaments are induced to collapse in living cells microinjected with monoclonal and polyclonal antibodies against tubulin. *J. Cell Biol.* 98:847–858.

Brady, S. T., M. Tytell, and R. J. Lasek. 1984. Axonal transport and axonal tubulin: biochemical evidence for cold stability. *J. Cell Biol.* 99:1716–1724.

Bré, M-H., T. Kreis, and E. Karsenti. 1987. Control of microtubule nucleation and stability in Madin-Darby Canine Kidney Cells: the occurrence of noncentrosomal, stable detyrosinated microtubules. *J. Cell Biol.* 105:1283–1296.

Bruckenstein, D. A., and D. Higgins. 1988*a*. Morphological differentiation of embryonic rat sympathetic neurons in tissue culture. I. Conditions under which neurons form axons but not dendrites. *Dev. Biol.* 128:324–336.

Bruckenstein, D. A., and D. Higgins. 1988*b*. Morphological differentiation of embryonic rat sympathetic neurons in tissue culture. II. Serum promotes dendritic outgrowth. *Dev. Biol.* 128:324–336.

Bulinski, J. C., and G. G. Gundersen. 1991. Stabilization and post-translational modification of microtubules during cellular morphogenesis. *Bioessays.* 13:285–293.

Ferreira, A., J. Busciglio, and A. Caceres. 1989. Microtubule formation and neurite growth in cerebellar macroneurons which develop in vitro: evidence for the involvement of microtubule-associated proteins MAP-1a, HMW-MAP2 and tau. *Dev. Brain Res.* 49:215–228.

Gundersen, G. G., and J. C. Bulinski. 1986. Microtubule arrays in differentiated cells contain elevated levels of a post-translationally modified form of tubulin. *Eur. J. Cell Biol.* 42:288–294.

Gundersen, G. G., S. Khawaja, and J. C. Bulinski. 1987. Postpolymerization detyrosination of α-tubulin: a mechanism for subcellular differentiation of microtubules. *J. Cell Biol.* 105:251–264.

Higgins, D., P. J. Lein, D. J. Osterhout, and M. I. Johnson. 1991. Tissue culture of mammalian autonomic neurons. *In* Culturing Nerve Cells. G. Banker and K. Goslin, editors. MIT Press, Cambridge, MA. 177–205.

Hollenbeck, P. J. 1989. The transport and assembly of the axonal cytoskeleton. *J. Cell Biol.* 108:223–227.

Jacobs, J. R., and J. K. Stevens. 1986. Changes in the organization of the neuritic cytoskeleton during nerve growth factor-activated differentiation of PC12 cells: a serial electron microscopic study of the development and control of neurite shape. J. Cell Biol. 103:895–906.

Joshi, H. C., and D. W. Cleveland. 1989. Differential utilization of β-tubulin isotypes in differentiating neurites. *J. Cell Biol.* 109:663–673.

Keith, C. H., and K. Blane. 1990. Sites of tubulin polymerization in PC12 cells. *J. Neurochem.* 54:1258–1268.

Kilmartin, J. V., B. Wright, and C. Milstein. 1982. Rat monoclonal anti-tubulin antibodies derived by using a new non-secreting rat cell line. *J. Cell Biol.* 93:576–582.

Kirschner, M., and T. Mitchison. 1986. Beyond self assembly: from microtubules to morphogenesis. *Cell.* 45:329–342.

Kreis, T. 1987. Microtubules containing detyrosinated tubulin are less dy-

namic. *EMBO (Eur. Mol. Biol. Organ.) J.* 6:2597–2606.
Lasek, R. J. 1986. Polymer sliding in axons. *In* The Cytoskeleton: Cell Function and Organization. *J. Cell Sci. Suppl.* 5:161–179.
Lasek, R. J. 1988. Studying the intrinsic determinants of neuronal form and function. *In* Intrinsic Determinants of Neuronal Form and Function. R. J. Lasek and M. M. Black, editors. Alan R. Liss, Inc., New York. 3–58.
LeBeau, J. M., M. H. Ellisman, and H. C. Powell. 1988. Ultrastructural and morphometric analysis of long-term peripheral nerve regeneration through silicon tubes. *J. Neurocytol.* 17:161–172.
Lim, S-S., P. J. Sammak, and G. G. Borisy. 1989. Progressive and spatially differentiated stability of microtubules in developing neuronal cells. *J. Cell Biol.* 109:253–263.
Lim, S-S., K. J. Edson, P. C. Letourneau, and G. G. Borisy. 1990. A test of microtubule translocation during neurite elongation. *J. Cell Biol.* 111: 123–130.
Mansfield, S. G., and P. R. Gordon-Weeks. 1991. Dynamic post-translational modification of tubulin in rat cerebral cortical neurons extending neurites in culture: effects of taxol. *J. Neurocytol.* 20:654–666.
Miller, S. 1991. Gene mapping by optical microscopy. American Laboratory Magazine, International Scientific Communications Inc., June 1991. 30.
Mitchison, T., and M. Kirschner. 1984. Dynamic instability of microtubule growth. *Nature (Lond.).* 312:237–242.
Mobley, W. C., A. Shenker, and E. M. Shooter. 1976. Characterization and isolation of proteolytically modified nerve growth factor. *Biochemistry.* 15:5543–5551.
Nixon, R. A. 1992. Slow axonal transport. *Curr. Opin. Cell Biol.* 4:8–14.
Okabe, S., and N. Hirokawa. 1988. Microtubule dynamics in nerve cells: analysis using microinjection of biotinylated tubulin into PC12 cells. *J. Cell Biol.* 107:651–664.
Okabe, S., and N. Hirokawa. 1990. Turnover of fluorescently labelled tubulin and actin in the axon. *Nature (Lond.).* 343:479–482.
Okabe, S., and N. Hirokawa. 1992. Differential behavior of photoactivated microtubules in growing axons of mouse and frog neurons. *J. Cell Biol.* 117:105–120.
Osborn, M., and K. Weber. 1982. Immunofluorescence and immunocytochemical procedures with affinity purified antibodies: tubulin containing structures. *In* Methods in Cell Biology. L. Wilson, editor. vol. 24, part A. 97–132.
Paddy, M. R., A. S. Belmont, H. Saumweber, D. Agard, and J. W. Sedat. 1990. Interphase nuclear envelope lamins form a discontinuous network that interacts with only a fraction of the chromatin in the nuclear periphery. *Cell.* 62:89–106.
Reinsch, S. S., T. J. Mitchison, and M. W. Kirschner. 1991. Microtubule polymer assembly and transport during axonal elongation. *J. Cell Biol.* 115: 365–379.
Robson, S. J., and R. D. Burgoyne. 1989. Differential localization of tyrosinated, detyrosinated, and acetylated α-tubulins in neurites and growth cones of dorsal root ganglion neurons. *Cell Motil. Cytoskeleton.* 12:273–282.
Schliwa, M., and J. J. van Blerkom. 1981. Structural interactions of cytoskeletal components. *J. Cell Biol.* 90:222–235.
Schulze, E., and M. Kirschner. 1986. Microtubule dynamics in interphase cells. *J. Cell Biol.* 102:1020–1031.
Schulze, E., D. J. Asai, J. C. Bulinski, and M. Kirschner. 1987. Post-translational modification and microtubule stability. *J. Cell Biol.* 105:2167–2177.
Sherwin, T., A. Schneider, R. Sasse, T. Seebeck, and K. Gull. 1987. Distinct localization and cell cycle dependence of COOH terminally tyrosinolated α-tubulin in microtubules of Trypanosoma brucei. *J. Cell Biol.* 104:439–446.
Sherwin, T., and K. Gull. 1989. Visualization of detyrosination along single microtubules reveals novel mechanisms of assembly during cytoskeletal duplication in trypanosomes. *Cell.* 57:211–221.
Soltys, B. J., and G. G. Borisy. 1985. Polymerization of tubulin in vitro: direct evidence for assembly onto microtubule ends and from centrosomes. *J. Cell Biol.* 100:1682–1689.
Tytell, M., M. M. Black, J. A. Garner, and R. J. Lasek. 1981. Axonal transport: each major rate component reflects the movement of distinct macromolecular complexes. *Science (Wash. DC).* 214:179–181.
Vallee, R. B. 1982. A taxol-dependent procedure for the isolation of microtubules and microtubule-associated proteins (MAPs). *J. Cell Biol.* 92:435–442.
Webster, D. R., G. G. Gundersen, J. C. Bulinski, and G. G. Borisy. 1987. Differential turnover of tyrosinated and detyrosinated microtubules. *Proc. Natl. Acad. Sci. USA.* 84:9040–9044.
Wehland, J., and M. C. Willingham. 1983. A rat monoclonal antibody reacting specifically with the tyrosylated form of α-tubulin. II. Effects on cell movement, organization of microtubules and intermediate filaments, and arrangement of Golgi elements. *J. Cell Biol.* 97:1476–1490.
Wehland, J., and J. Weber. 1987. Turnover of the carboxy-terminal tyrosine of α-tubulin and means of reaching elevated levels of detyrosination in living cells. *J. Cell Sci.* 88:185–203.
Wehland, J., M. C. Willingham, and I. V. Sandoval. 1983. A rat monoclonal antibody reacting specifically with the tyrosylated form of α-tubulin. I. Biochemical characterization, effects on microtubule polymerization *in vitro* and microtubule polymerization and organization in vivo. *J. Cell Biol.* 97: 1476–1490.
Weiss, P. A., and H. B. Hiscoe. 1948. Experiments on the mechanism of nerve growth. *J. Exp. Zool.* 107:315–396.